Tuning the band gap of the CIGS solar buffer layer $Cd_{1-x}Zn_xS$ (x=0—1) to achieve high efficiency*

TAN Zhiyuan, XUE Yuming, DAI Hongli, WANG Luoxin, HU Xiaofeng, and BAI Xin**

Institute of New Energy Intelligence Equipment, School of Integrated Circuit Science and Engineering, Tianjin University of Technology, Tianjin 300384, China

(Received 27 December 2022; Revised 8 July 2023)

To evaluate the impact of zinc sulfate ($ZnSO_4$) concentration on the structural properties of the films, $Cd_{1-x}Zn_xS$ thin films were formed on glass substrates using chemical bath deposition (CBD) in this study. The effect of $ZnSO_4$ precursor concentration on the surface morphology, optical properties, and morphological structure of the $Cd_{1-x}Zn_xS$ films was investigated. To study the impact of zinc doping content on the performance metrics of $Cu(In_{1-x}Ga_x)Se_2$ (CIGS) cells in the experimental group and to improve the buffer layer thickness, simulations were run using one-dimensional solar cell capacitance simulator (SCAPS-1D) software.

Document code: A **Article ID:** 1673-1905(2024)02-0100-7

DOI https://doi.org/10.1007/s11801-024-2222-6

CdS has been investigated for many years as a buffer layer for heterojunction solar cells because it is an N-type direct band gap semiconductor material with strong transparency in the visible region and an optical band gap of 2.43 eV[1]. However, the short wave is prevented in the absorption layer by the narrow optical band gap of CdS. By the way, cadmium is a toxic substance that is harmful to the body. ZnS is an environmentally friendly N-type semiconductor compound with an optical band gap of 3.71 eV[2] and good short-wave transmittance and has been widely considered as a replacement for CdS. Due to the weak lattice of CdZnS, solar cells utilizing ZnS as a buffer layer have a significantly lower efficiency than solar cells using CdS as a buffer film. By adjusting the concentration of Zn ions, CdZnS can be formed between CdS and ZnS, resulting in a good lattice match and optical transmittance[3], thus improving the performance of the solar cell. On the other hand, it can reduce the use of the toxic substance cadmium.

There are numerous techniques for creating thin films of CdS, ZnS, and CdZnS, including atomic layer deposition[4], thermal evaporation[5], and chemical bath deposition (CBD)[6]. The CBD method is used because of its low cost and the fact that it does not require vacuum conditions[7]. The procedure is straightforward and the deposition settings are simpler to manage at the same time[8]. By using the microwave-assisted CBD process, MAHDI et al[9] created CdZnS thin films with an optical band gap of 2.66 eV. The films are suitable as buffer materials for solar cells because of their high transmittance, and homogeneous, and compact surfaces.

In this study, $Cd_{1-x}Zn_xS$ thin films with comparable photoelectronic characteristics to CdS were made using the CBD approach employing zinc sulfate ($ZnSO_4$) as a zinc source, cadmium, and zinc precursors as raw ingredients. The morphology, structure, and optical properties of $Cd_{1-x}Zn_xS$ films were examined, and they were compared to CdS films as well as other $Cd_{1-x}Zn_xS$ films made under similar conditions. The different band gaps and thicknesses of the buffer layers were also verified in the simulation software one-dimensional solar cell capacitance simulator (SCAPS-1D) to obtain optimal buffer layer data, which is useful for the preparation of solar cells.

A ternary mixing system with $Cd_{1-x}Zn_xS$ as a buffer was studied. It has been reported[9] that in $Cu(In_{1-x}Ga_x)Se_2$ (CIGS) solar cells, the $Cd_{1-x}Zn_xS$ buffer layer has improved in terms of open circuit voltage (V_{OC}) and short circuit current (J_{SC}) compared to conventional CdS. By depositing $Cd_{1-x}Zn_xS$ films using the CBD method, the aim is to enhance the performance of the films in all aspects. In addition, we compared CdS films generated in the same environment and explored the effect of different amounts of zinc added to x on the morphology, structure, and optical properties of the $Cd_{1-x}Zn_xS$ buffer layer.

In this investigation, the CBD technique was used to deposit $Cd_{1-x}Zn_xS$ films on indium tin oxide (ITO) substrates. The bottom plate should first be thoroughly cleaned with hydrochloric acid, an ultrasonic cleaning solution, and pure water before being dried with nitrogen. They were then put into beakers containing in order, $CdSO_4$ (0.007 M), $(NH_4)_2SO_4$ (0.01 M), various $ZnSO_4$

* This work has been supported by the Science and Technology Innovation Development Program (No.70304901).
** E-mail: orwellx@tjut.edu.cn

concentrations, and the proper volumes of deionized water. It was then put in a bath of water that was always the same temperature after being thoroughly stirred. The reaction solution contains between 0.01 M and 0.03 M of $ZnSO_4$, and a set of films without doped elemental zinc were created for comparison. The reaction starts to create a yellow precipitate in the beaker after 35 min in a water bath that has been heated to 88 °C. Ammonia (25%) and $SC(NH_2)_2$ (0.01 M) were added consecutively, the timing was begun, and stirring was done every 5 min. Take out the beaker, thoroughly clean the sample, and then dry it with nitrogen gas.

In this experiment, if Cd^{2+}, Zn^{2+}, and S^{2-} are present in the solution, they precipitate rapidly because the dissolved products are too small, which in turn would affect the film growth. Cd^{2+} and Zn^{2+} react with NH_4^+ to form a stable complex and then with S^{2-} to control the deposition rate and thus improve the quality of the film. During deposition, the ensuing chemical processes Eqs.(1)—(4) take place.

$$Zn^{2+}+Cd^{2+}+4OH^- \leftrightarrow Zn(OH)_2^-+Cd(OH)_2^-, \quad (1)$$

$$Zn(OH)_2+Cd(OH)_2+8NH_4OH \rightarrow [Zn(NH_3)_4]^{2+}+[Cd(NH_3)_4]^{2+}+8H_2O+4OH^-, \quad (2)$$

$$SC(NH_2)_2+2OH^- \rightarrow S^{2-}+2H_2O+CH_2N_2, \quad (3)$$

$$[Cd(NH_3)_4]^{2+}+[Zn(NH_3)_4]^{2+}+S^{2-} \rightarrow Cd_{1-x}Zn_xS+\text{waste}. \quad (4)$$

In this work, the crystal structure of the film was analyzed by X-ray diffraction (XRD). The element composition, surface morphology, and film content analysis use a scanning electron microscope (SEM) and an energy dispersion spectrometer (EDS). The absorbance and transmittance of the films were measured with a UV-visible-near-infrared spectrophotometer (TP720) in the wavelength range of 300—800 nm, and then the band gap was calculated.

The structure and properties of $Cd_{1-x}Zn_xS$ films were analyzed by XRD. The diffraction pattern is shown in Fig.1(a). When a zinc precursor solution is not present, the CdS film exhibits diffraction peaks at 2θ=26.54°. The XRD pattern within 25°—28° variations in diffraction peaks become visible. As seen in Fig.1(b), the diffraction peak started shifting constantly at about 2θ=26.7° when zinc precursor was added, and the single peak there is thought to be the hexagonal phase $Cd_{1-x}Zn_xS$, which is consistent with earlier report[10]. As the zinc concentration of the reaction solution increases, when zinc is doped into the CdS crystal structure, the sharpest peak location moves because the lattice constant of $Cd_{1-x}Zn_xS$ is less than that of CdS[11], causing Cd^{2+} to be replaced by Zn^{2+} in its lattice position, which results in a reduction in lattice constants and lattice plane distances. Therefore, the diffraction peak of $Cd_{1-x}Zn_xS$ corresponds to an increase in 2θ.

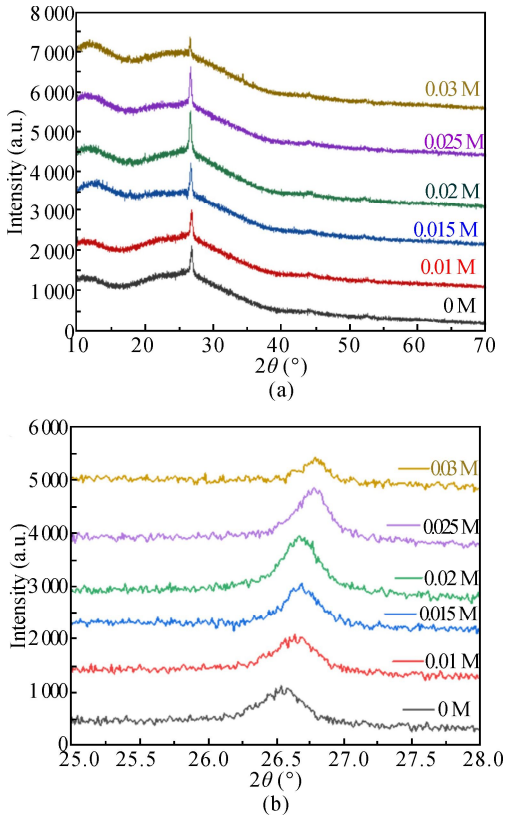

Fig.1 XRD characterization of cadmium sulfate prepared from different concentrations of $ZnSO_4$: (a) 10°—70°; (b) 25.0°—28.0°

Except for the diffraction peak's displacement, the main diffraction peak's height decreases as the concentration of zinc salt rises while its width widens. This indicates that the crystallinity increases with the increase of zinc content and the higher the zinc content, the lower the crystallinity. Extrapolating from the above-mentioned reaction mechanism, this occurs because in the reaction solution, greater concentrations of Zn^{2+} preferentially occupy NH_3 to create stable complexes, i.e., they prevent the formation of Cd^{2+} complexes with NH_3, resulting in less binding of cadmium ions to the sulphur precursors, so the film diffraction peaks decrease[12].

Fig.2 demonstrates $Cd_{1-x}Zn_xS$ thin film electron microscopy photos, demonstrating that all samples produced a thin film and that nanoparticles were dispersed randomly across it. At $ZnSO_4$ levels of 0 M, 0.01 M, and 0.015 M (Fig.2(a)—(c)), there is no agglomeration and the films are of good quality with no pores present. A few pore flaws first develop in the film at 0.02 M $ZnSO_4$, and these defects keep becoming worse at 0.025 M and 0.03 M $ZnSO_4$ (Fig.2(d)—(f)). The film's growth rate was slowed down by the expansion of its pores[13], and it also got thinner.

The composition and film thickness of $Cd_{1-x}Zn_xS$

produced by different concentrations of $ZnSO_4$ under this experiment were examined by EDS and bench scale respectively, and the obtained elemental percentages and thickness values are listed in Tab.1. The analysis of the table shows that the reaction solution, the increase in the concentration of Zn^{2+} led to the relevant reaction moving in the positive direction, resulting in the formation of $Cd(OH)_2$, $Zn(OH)_2$, and S^{2-} in solution at a higher rate than that of Zn^{2+}, Cd^{2+}, and S^{2-} to generate $Cd_{1-x}Zn_xS$ films. This accelerated the rate of metal ion release. $Zn(OH)_2$ precipitates more quickly than $Cd_{1-x}Zn_xS$ films are formed from Zn^{2+}, Cd^{2+}, and S^{2-}. Therefore, more Zn is doped into the CdS crystals. However, the pace of film growth is slowing[14], and the films are getting thinner and less thick with holes appearing. This corresponds to the defects observed in the SEM images.

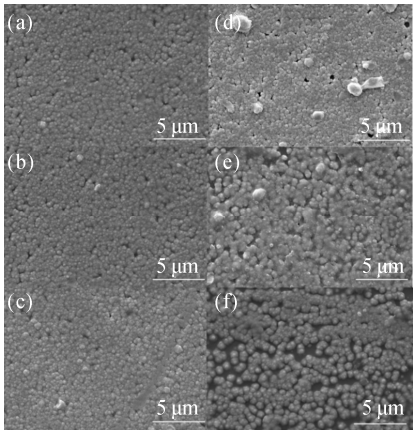

Fig.2 SEM images of different concentrations of Zn-Cd-S films: (a) 0 M; (b) 0.01 M; (c) 0.015 M; (d) 0.02 M; (e) 0.025 M; (f) 0.03 M

Tab.1 Thicknesses of cadmium sulphur and zinc films at different concentrations

$ZnSO_4$ concentration (M)	at% (S: Zn: Cd)	Film thickness (nm)
0	42.74: 0.00: 57.26	110.2
0.01	36.00: 8.56: 55.44	84.7
0.015	28.95: 16.07: 54.97	73.6
0.02	26.17: 20.46: 53.37	66.2
0.025	24.32: 24.51: 51.17	59.1
0.03	23.61: 31.22: 45.17	40.9

Films with fewer surface holes and better densities are more appropriate for use in thin film buffer layers because holes increase the likelihood of carrier compounding and decrease photovoltaic conversion efficiency[15].

The optical performance of the thin film obtained in the experiment was investigated with a UV-visible-near-infrared spectrophotometer. From the absorbance shown in Fig.3(a), these thin films have high absorbance for light below 500 nm and drop sharply between 300 nm and 350 nm. As a result, it was found that the absorbance of $Cd_{1-x}Zn_xS$ film to Cd film increased with the concentration of Zn^{2+} at the same wavelength.

A very translucent film must be created to ensure that the buffer layer allows the most light through to the absorber layer. Fig.3(b) displays the experiment's film transmittance. In the range of 500—800 nm, the average light transmittance is 70%—85%. As the concentration of Zn^{2+} increases, the films can reach 85% transmission at 500 nm with the superior optical performance. In addition, as the Zn content in the film increases, there is a significant blue shift in the absorption edge.

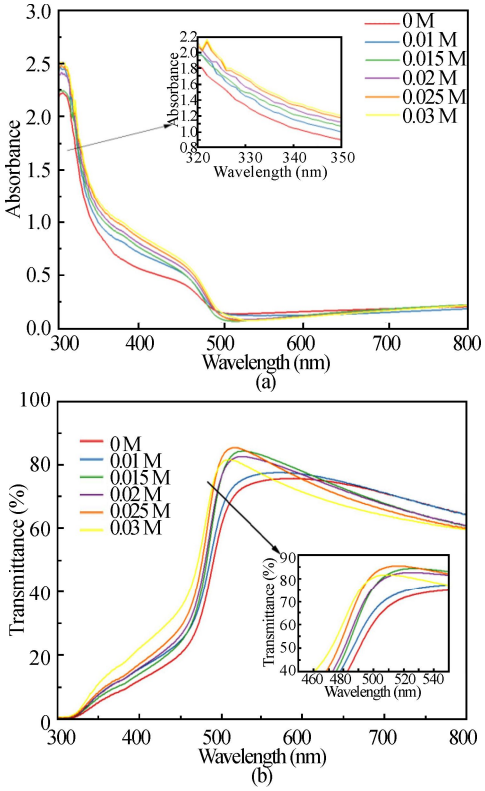

Fig.3 (a) Absorbance and (b) transmittance versus wavelength for different concentrations of ZnCdS films

The optical band gap and absorption coefficient of $Cd_{1-x}Zn_xS$ films conform to Tauc Eq.(5)[16]

$$(\alpha hv)^n = A(hv - Eg). \tag{5}$$

The photon energy, absorption coefficient, light band of the thin film, and constant A are all included in the equation above. Since $Cd_{1-x}Zn_xS$ is a semiconductor with a direct band gap, index n equals 2. The $(\alpha hv)^2$-hv variance curve is tangent to the adjusted variance curve and intersects the horizontal axis. The film's banned light band is located along the X-axis, which crosses the horizontal axis. It resembles Fig.4.

The band gap measurements and atomic compositions of the $Cd_{1-x}Zn_xS$ film produced in this experiment are displayed in Tab.2. It is seen that as the concentration of $ZnSO_4$ rises, the films' bandwidth steadily increases. The changes in the strip gap correspond to changes in the EDS

measurement of zinc content. The increasing trend in band gap values confirmed the replacement of zinc with the $Cd_{1-x}Zn_xS$ structure.

Further investigation has revealed a functional link between the band gap and the zinc content x. For instance, the band gap value and x have a relationship[17] that fulfills Eq.(6).

$$E_g(x) = kx^2 + (E_{g(ZnS)} - E_{g(CdS)} - k)x + E_{g(CdS)}. \quad (6)$$

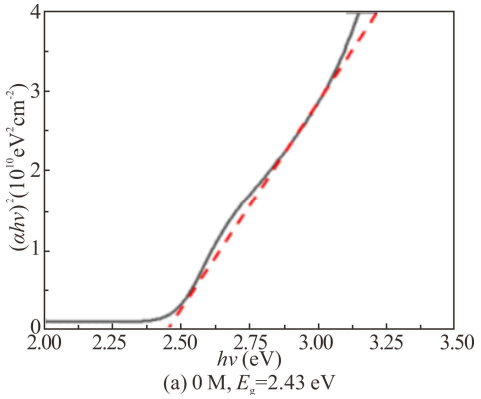

(a) 0 M, E_g=2.43 eV

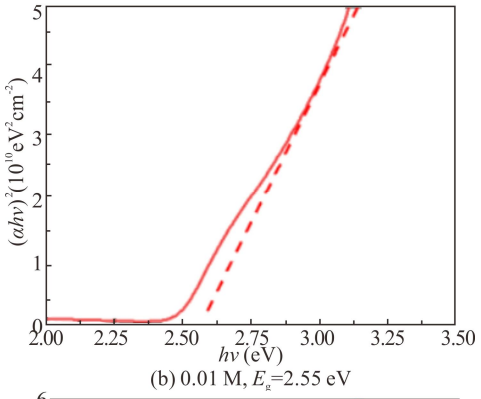

(b) 0.01 M, E_g=2.55 eV

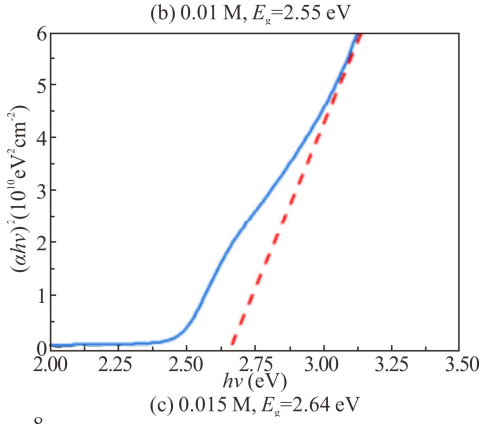

(c) 0.015 M, E_g=2.64 eV

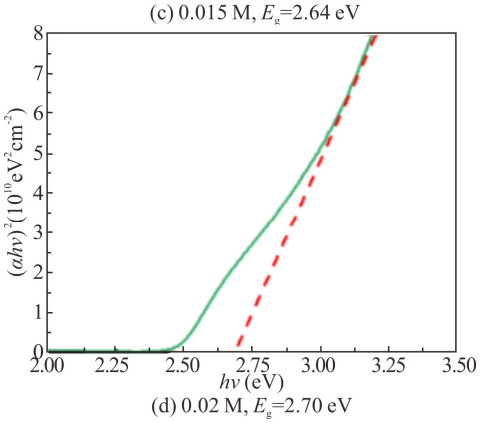

(d) 0.02 M, E_g=2.70 eV

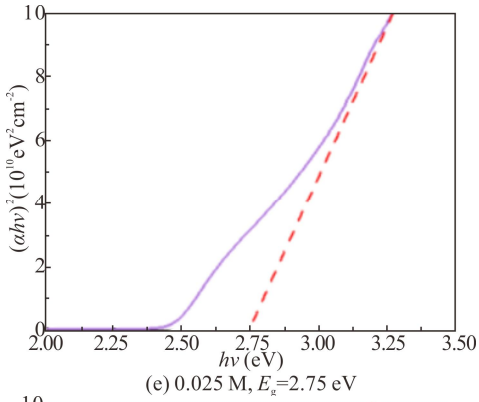

(e) 0.025 M, E_g=2.75 eV

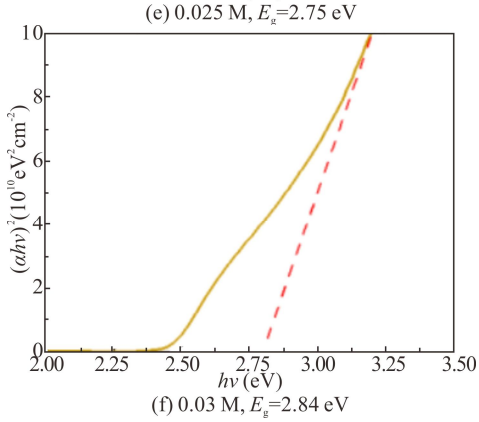

(f) 0.03 M, E_g=2.84 eV

Fig.4 Band gap energy diagrams for different concentrations of Zn-Cd-S films

Tab.2 Elemental contents and band gaps of different concentrations of S-Zn-Cd films

$ZnSO_4$ concentration (M)	at% (S: Zn: Cd)	Zn/ Cd+Zn	$Cd_{1-x}Zn_xS$	E_g (eV)
0	42.74: 0.00: 57.26	0.000	CdS	2.43
0.01	36.00: 8.56: 55.44	0.133	$Cd_{0.87}Zn_{0.13}S$	2.55
0.015	28.9: 16.07: 54.97	0.226	$Cd_{0.78}Zn_{0.22}S$	2.64
0.02	26.1: 20.46: 53.37	0.277	$Cd_{0.73}Zn_{0.27}S$	2.70
0.025	24.3: 24.51: 51.17	0.323	$Cd_{0.68}Zn_{0.32}S$	2.75
0.03	23.6: 31.22: 45.17	0.408	$Cd_{0.6}Zn_{0.4}S$	2.84

The band gap values for ZnS and CdS are $E_{g(ZnS)}$ and $E_{g(CdS)}$, respectively, where k is the curve coefficient. In this experiment, the band gap value E_g and the x of the $Cd_{1-x}Zn_xS$ film have a nonlinear connection that may be represented as

$$E_g(x) = 0.31x^2 + 0.92x + 2.43. \quad (7)$$

The resulting equation states that the $Cd_{1-x}Zn_xS$ film's band gap value changes from 0 to 1 and that the optical band gap of the film grows as zinc content increases. The

energy bands of the buffer and absorption layers of the film can be matched by correctly altering the zinc content, it increases the film's absorbance and improves its photoelectric efficiency.

Numerical simulations are an important tool for understanding the physical mechanisms of devices, testing the feasibility of proposed cell structures, and forecasting solar cell performance before commercial production. The SCAPS-1D program, version 3.3.10, was employed in this work. SCAPS was initially created for CdTe and CIGS solar cells, which are polycrystalline thin-film devices. The program uses Poisson's equation along with the hole and electron continuity equations to compute one-dimensional steady-state energy band diagrams, complex distributions, and carrier transport as Eqs.(8)—(10).

$$\frac{\mathrm{d}^2}{\mathrm{d}x^2}\psi(x)=\frac{e}{\varepsilon_0\varepsilon_\mathrm{r}}\left(p(x)-n(x)+N_\mathrm{D}-N_\mathrm{A}+\rho_\mathrm{p}-\rho_\mathrm{n}\right), \quad (8)$$

$$\frac{\mathrm{d}}{\mathrm{d}x}J_\mathrm{n}(x)=G(x)-R(x), \quad (9)$$

$$\frac{\mathrm{d}}{\mathrm{d}x}J_\mathrm{p}(x)=G(x)-R(x), \quad (10)$$

where e is a charge, p and n are hole and electron concentrations, N_D is the charged impurity of the applicator, ε_r is relative, ε_0 is the vacuum dielectric constant, and ψ is the electrostatic potential, N_A is the type of acceptor, ρ_p and ρ_n are hole and electron distributions, J_n and J_p are electron and hole current densities, and $G(x)$ and $R(x)$ are charge generation and complexation rates, respectively.

In this study, the SCAPS-1D software was used to verify the feasibility of the experimentally prepared $Cd_{1-x}Zn_xS$ film as a buffer layer for solar cells like CIGS, after which the optimal thickness of the new buffer layer was determined and the performance of the optimized $Cd_{1-x}Zn_xS$ film in CIGS solar cells was monitored. To validate the experimental results, the mature CIGS (Mo/CIGS/CdS/i-ZnO) structure was used for this simulation and the experimental results of $Cd_{1-x}Zn_xS$ were used instead of CdS, and the simulation model shown in Fig.5. All simulations have been carried out in the AM 1.5 spectrum and at a light intensity of 1 000 W/m^2 and a temperature of 300 K. Typical thickness of each layer is taken from different reports[18,19] and Tab.3 records the simulation parameters.

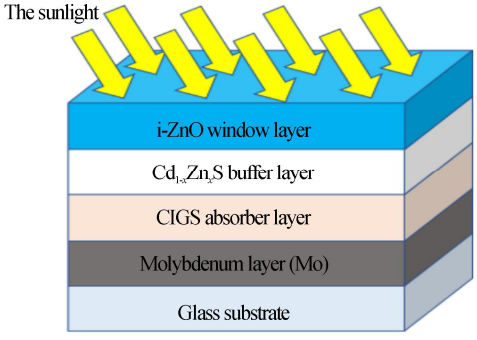

Fig.5 Structure of a CIGS solar cell

Tab.3 Simulation parameters

Parameter	CIGS	i-ZnO	$Cd_{1-x}Zn_xS$
Thickness (nm)	2 000	120	Experiment
E_g (eV)	1.2	3.3	Experiment
χ (eV)	4.6	4.4	4.26
ε_r	9	9	9.23
N_c (cm^{-3})	2.2×10^{18}	2.0×10^{18}	2.1×10^{18}
N_v (cm^{-3})	1.5×10^{19}	2.0×10^{19}	1.7×10^{19}
μ_e (cm^2/Vs)	100	100	70
μ_h (cm^2/Vs)	12.5	25	20
N_D (cm^{-3})	-	1.0×10^{18}	1.0×10^{16}
N_A (cm^{-3})	2.0×10^{17}	1.0×10^{18}	-

The *J-V* curves of the experimental data are shown in Fig.6, which corresponds to different $ZnSO_4$ concentrations. From the graph, it can be seen that the V_OC varies slightly but can be considered constant. When $ZnSO_4$ was not added, i.e., the starting current density J_SC of CdS was 35.652 mA/cm^2 when 0.03 M $ZnSO_4$ was added, the current density increased to 35.981 mA/cm^2. From the experimental results, it is known that the buffer layer forbidden bandwidth is gradually increasing, which makes the absorber layer absorb more photons. The simulation results of Zn^{2+} concentration on cell performance metrics, such as V_OC, J_SC, filling factor (*FF*) and efficiency, are listed in Tab.4. As a result, an increase in the number of carriers generated in the absorber layer results in an increase in the photogenerated current. When 0.015 M is added, corresponding to the $Cd_{0.78}Zn_{0.22}S$ compound, the efficiency reaches a maximum of 23.25%. And from the above, it is known that this concentration has good film properties. Therefore, the $Cd_{0.78}Zn_{0.22}S$ prepared at this concentration can be used as a subsequent research material for the buffer layer of CIGS solar cells.

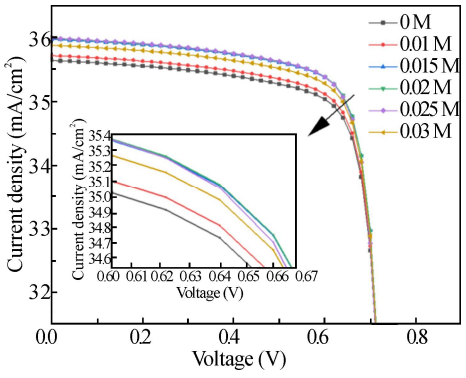

Fig.6 Experimental *J-V* curves

The simulation continues with the optimal parameters of $Cd_{0.78}Zn_{0.22}S$ film and varies the thickness in the range of 20—80 nm to investigate the effect of buffer layer thickness on the cell performance. As shown in Fig.7(a), the *J-V* curves of the cell with different thicknesses of buffer layers are shown. As can be seen from the figure, the thickness increases from 20 nm to 50 nm, the J_SC gradually rises, and after 50 nm, it gradually decreases. Here the

buffer layer band gap is 2.64 eV, which makes the photon energy enter the absorber layer lower than this energy.

Tab.4 Simulation results for different concentrations of $ZnSO_4$ precursors

Concentration (M)	V_{oc} (V)	J_{sc} (mA/cm^2)	*FF* (%)	Efficiency (%)
0	0.780 7	35.642 5	82.71	23.01
0.01	0.780 6	35.714 3	82.73	23.06
0.015	0.780 7	35.876 1	82.76	23.25
0.02	0.780 7	35.969 4	82.74	23.24
0.025	0.780 6	35.981 3	82.72	23.18
0.03	0.780 8	35.986 2	82.43	23.16

The quantum efficiency (*QE*) is significantly influenced by the thickness of the buffer layer, notably in the blue UV area, as seen in Fig.7(b). The findings demonstrate that as buffer layer thickness grows, the *QE* first rises and then falls, reaching its maximum at a buffer layer thickness of 50 nm. This is due to the fact that short-wave photons are absorbed close to the surface, and a buffer layer that is thinner and closer to the surface is better able to collect short-wave photons than a thicker buffer layer. It is important to note that shorter wavelength photons are absorbed in greater distances from the window to the absorbing layer as the buffer layer thickness increases. As a result of having more defect traps than a thinner layer, a thicker buffer layer is less efficient[20]. Therefore, this simulation concluded that the optimum thickness for $Cd_{0.78}Zn_{0.22}S$ is 50 nm, at which the V_{OC}, J_{SC}, *FF* and efficiency are 0.782 6 mV, 38.197 mA/cm^2, 82.95%, and 24.5%, respectively.

The XRD results demonstrate that the Zn doping causes the diffraction peaks to begin hysteresis. If the Zn content is higher, the crystallinity of the film is significantly poorer. The morphological results show that when the proportion of Zn in the film increases, the growth rate decreases, the thickness becomes thinner, the denseness degrades, the porosity increases and the film grows slowly. The zinc concentration and optical band value of the film are changed by the ultraviolet

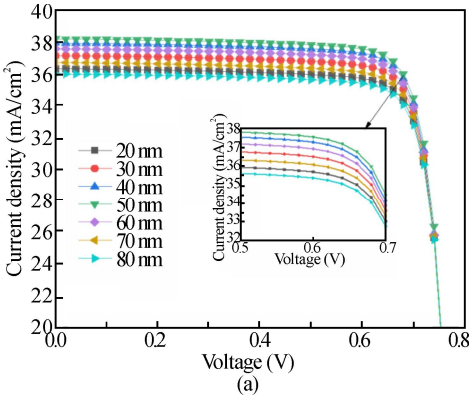

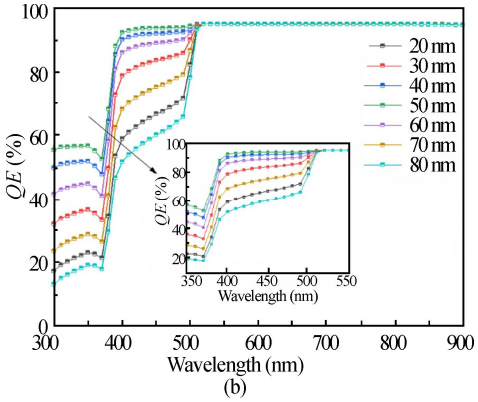

Fig.7 (a) *J-V* and (b) *QE* curves of CIGS thin film cells with different buffer layer thicknesses

test. Higher optical band gap values, greater absorption, and permeability are all characteristics of the film, and the equation $E_g(x)=0.31x^2+0.92x+2.43$ holds for both the optical band gap and zinc concentration. The findings demonstrate that 50 nm is the optimal buffer layer thickness and that 0.015 M $ZnSO_4$ is the best concentration for creating the $Cd_{1-x}Zn_xS$ buffer layer. Future design and fabrication of buffers for CIGS solar cells will use this optimization work as a guide.

Ethics declarations

Conflicts of interest

The authors declare no conflict of interest.

References

[1] ABZA T, AMPONG F K, HONE F G, et al. Preparation of cadmiumzinc sulfide ($Cd_{1-x}Zn_xS$) thin films from acidic chemical baths[J]. Thin solid films, 2018, 666: 28.

[2] BARMAN B, BANGERA K V, SHIVAKUMAR G K. A comprehensive study on the structural, morphological, compositional and optical properties of $Zn_xCd_{1-x}S$ thin films[J]. Materials research express, 2020, 6(12): 126441-126441.

[3] ZELLAGUI R, DEHDOUH H, ADNANE M, et al. $Cd_xZn_{1-x}S$ thin films deposited by chemical bath deposition (CBD) method[J]. Optik, 2020, 207: 164377.

[4] PUROHIT A, PATEL S L, CHANDER S, et al. Substrate evolution to microstructural and optoelectrical properties of evaporated CdS thin films correlated with elemental composition[J]. Acta metallurgica sinica (English letters), 2021, 34(9): 1307-1316.

[5] XUE Y, ZHANG S, SONG D, et al. Effect of concentration of cadmium sulfate solution on structural, optical and electric properties of $Cd_{1-x}Zn_xS$ thin films[J]. Journal of semiconductors, 2021, 42(11): 112101.

[6] XIE X, XUE Y, LV C, et al. Tuning zinc doping content to optimize optical and structural properties of $Cd_{1-x}Zn_xS$ buffer layers[J]. Optoelectronics letters, 2023, 19(1): 25-30.

[7] ZELLAGUI R. $Cd_xZn_{1-x}S$ thin films deposited by chemical bath deposition (CBD) method[J]. Optik, 2020, 207(C): 164377-164377.

[8] WANG L, XUE Y, WANG Z, et al. Effects of ammonia concentration on morphology, composition and optical properties of $ZnO_{1-x}S_x$ thin films of $Cu(In,Ga)Se_2$ solar cells[J]. Optoelectronics letters, 2022, 18(4): 215-221.

[9] MAHDI M A, HASSAN J J, HASSAN Z, et al. Growth and characterization of $Zn_xCd_{1-x}S$ nanoflowers by microwave-assisted chemical bath deposition[J]. Journal of alloys and compounds, 2012, 541: 227-233.

[10] MUNNA F T, SELVANATHAN V, SOBAYEL K, et al. Diluted chemical bath deposition of CdZnS as prospective buffer layer in CIGS solar cell[J]. Ceramics international, 2021, 47: 11003-11009.

[11] ZHANG L M. Influence of ammonia concentration on the structural, composition and optical properties of CdZnS thin films[J]. Materials science in semiconductor processing, 2019, 104(C): 104650-104650.

[12] MUNNA F T. Effect of zinc doping on the optoelectronic properties of cadmium sulphide (CdS) thin films deposited by chemical bath deposition by utilizing an alternative sulphur precursor[J]. Optik, 2020, 218: 165197.

[13] SMAIRI S. Elaboration and characterization of cadmium sulfide (CdS) thin films prepared by chemical bath deposition (CBD)[J]. Materials today: proceedings, 2022, 66: 112-115.

[14] ERTHRK K. Optical and structural characteristics of electrodeposited $Cd_{1-x}Zn_xS$ nanostructured thin films[J]. Optical materials, 2021, 114.

[15] JRAD A. Investigation of molybdenum dopant effect on ZnS thin films: chemical composition, structural, morphological, optical and luminescence surveys[J]. Materials science in semiconductor processing, 2021, 130: 105825.

[16] XUE Y M. Effect of concentration of cadmium sulfate solution on structural, optical and electric properties of $Cd_{1-x}Zn_xS$ thin films[J]. Journal of semiconductors, 2021, 42(11): 6.

[17] SOBAYEL K. A comprehensive defect study of tungsten disulfide (WS2) as electron transport layer in perovskite solar cells by numerical simulation[J]. Results in physics, 2019, 12: 1097-1103.

[18] HOSSAIN T, SOBAYEL M K, MUNNA F T, et al. Tuning the bandgap of $Cd_{1-x}Zn_xS$ (x=0~1) buffer layer and CIGS absorber layer for obtaining high efficiency[J]. Superlattices and microstructures, 2022, 161: 107100.

[19] ALBI A. Effects of temperature, thickness, electron density and defect density on ZnS based solar cells: SCAPS-1D simulation[J]. Materials today, 2022, 66: 116-121.

[20] LI W. Numerical analysis of the back interface for high-efficiency wide band gap chalcopyrite solar cells[J]. Solar energy, 2019, 180: 207-215.